



Monte Carlo simulation of the topological quantities in fractional quantum Hall systems

Yi Yang  and Zi-Xiang Hu ^{*}

*Department of Physics and Chongqing Key Laboratory for Strongly Coupled Physics,
Chongqing University, Chongqing 401331, People's Republic of China*



(Received 19 December 2022; accepted 21 March 2023; published 29 March 2023)

Generally speaking, for a fractional quantum Hall (FQH) state, the electronic occupation number for each Landau orbit could be obtained by numerical methods such as exact diagonalization, density matrix renormalization group, matrix product state, or algebraic recursive schemes (Jack polynomial). In this paper, we apply a Metropolis Monte Carlo method to calculate the occupation numbers of several FQH states in cylinder geometry. The convergent occupation numbers for more than 40 particles are used to verify the chiral bosonic edge theory and determine topological quantities from momentum polarization or dipole moments. The guiding center spin, central charge, and topological spin of different topological sectors are consistent with theoretical values and other numerical studies. In particular, we obtain the topological spin of a $e/4$ quasihole in Moore-Read and 331 states. Lastly, we calculate the electron edge Green's functions and analyze the position dependence of the non-Fermi liquid behavior.

DOI: [10.1103/PhysRevB.107.115162](https://doi.org/10.1103/PhysRevB.107.115162)

I. INTRODUCTION

Since the discovery of the fractional quantum Hall (FQH) effect [1,2], its rich physical connotations and novel topological properties have attracted extensive attention. Different from the integer quantum Hall (IQH) state, the FQH state is embedded with quantum topological order which manifests novel properties including fractional charge excitation, fractional statistics, topological ground state degeneracy, gapless chiral edge excitation, and topological entanglement entropy, etc. [3–6]. It is worth mentioning that the fractional statistics of the anyonic excitations in FQH have been recently identified experimentally by either the Fabry-Pérot interference or anyon collisions near the quantum point contacts (QPCs) [7–11]. The quantum Hall bulk is an incompressible insulator with which it is difficult to provide measurable signals in experiments. However, its conducting gapless edge mode provides a tool to detect the topological properties due to the bulk-edge correspondence mechanism [3,12]. In the early 1990s, the physics of edge excitation was considered extremely important to the FQH [4,13–15]. It is known that most of the FQH edges can be treated as a chiral Luttinger liquid (χ LL) instead of a noninteracting Fermi liquid [16]. In experiments, one can measure the non-Fermi liquid behavior via a nonlinear $I \propto V^\alpha$ relation in the tunneling experiment from Fermi liquid to FQH liquid. The Tomonaga-Luttinger (TL) exponent α could be calculated from the edge Green's function $G(|\vec{r}_1 - \vec{r}_2|) = \langle \psi^\dagger(\vec{r}_1)\psi(\vec{r}_2) \rangle \propto |\vec{r}_1 - \vec{r}_2|^{-\alpha}$. The edge electron propagator also describes the entanglement of two particles on the edge. Wen's effective theory [4] demonstrated that the spatial decay of the electron propagator involves a non-Fermi-liquid exponent $\alpha = q$ for $\nu = 1/q$ Laughlin state

and $\alpha = 3$ for the Moore-Read (MR) state and 331 state. For a realistic system with Coulomb interaction, the values of α are not that universal. This has attracted a lot of theoretical and experimental attention [16–28], such as the influence of edge reconstruction, sample qualities, and the emergence of a neutral mode. Recently, it was verified that the FQH in suspended graphene could avoid those obstructive factors and realize the universal edge physics [29–32]. Similarly, the occupation numbers near the edge obey $\lim_{k \rightarrow \text{edge}} n_k \propto k^\beta$ in the continuum limit, as predicted by chiral boson edge theory [33]. At the same time, the information of the bulk magnetoroton excitation has been claimed to be embodied in the oscillation of the occupation numbers near the edge [34].

In a correlated FQH system, the density deviates from the bulk filling $\rho = \frac{\nu}{2\pi l_B^2}$ near the edge and thus results in an extra intrinsic dipole moment which is related to the guiding-center Hall viscosity [35–37]. It is worth mentioning that Hall viscosity is characterized by a rational number and a metric tensor that defines distances on an incompressibility length scale, and its magnitude provides a lower bound to the coefficient of the $O(q^4)$ small- q limit of the guiding center structure factor. The Hall viscosity is also related to the momentum polarization [38,39] of the system while rotating half of the system and maintaining another half invariant. In fact, momentum polarization is the subleading term of the average value of a partial translation operator. Therefore, the calculation of the intrinsic dipole moment, or momentum polarization, averages the momentum operator of a subsystem in a bipartition. Interestingly, topological quantities of the FQH state, such as guiding-center spin, central charge, and topological spin of the quasiparticle excitation, could also be determined from the coefficients and corrections of the momentum polarization [35,40–42]. The guiding-center spin is related to the nondissipative response of the metric perturbation in FQH liquids. Its coupling with the geometric

^{*}zxhu@cqu.edu.cn

curvature of the underlying manifold gives the topological shift of the FQH states in spherical geometry. The topological spin and central charge are the elements of a modular- T matrix that are used to describe the topological order of the FQH state [43]. Meanwhile, the central charge determines the heat current $I_E = \frac{\pi}{6} c T^2$ at a given temperature T [44] and is also related to the gravitational anomaly of the edge [45].

In numerical calculations, the density fluctuations of the quantum Hall edge affect several Landau orbits, and the range of its influence becomes larger for small bulk density. For example, the edge of the $\nu = 1/5$ Laughlin state affects more orbits than that of the $\nu = 1/3$ Laughlin state. Moreover, in the case of realistic long-range Coulomb interaction, the edge oscillates deeper into the bulk than the short-range model interaction. A criterion for obtaining a complete profile of the edge state is that the bulk density should be stable at the filling factor $\nu/2\pi l_B^2$. This is usually beyond the reach of exact diagonalization or the Jack polynomial, which are limited by the small size of Hilbert space. The inaccurate momentum polarization calculation of the small system size cannot give convergence of physical quantities or even incorrect results at some time. The developments to solve this problem were the density-matrix renormalization group (DMRG) [34,42] and the infinite DMRG based on the Matrix product state representation [41]. In this paper, we develop the Monte Carlo simulation method in cylinder geometry to calculate occupation numbers for several FQH states. From these occupation numbers, we explore momentum polarization and its related topological quantities with high accuracy. The edge Green's function is also calculated for a large system, and the parameter of the chiral Luttinger liquid theory is determined with higher accuracy than previous studies. Comparing to the iDMRG method [41], which deals with an infinite cylinder with translational symmetry. The topological quantities were extrapolated from the momentum polarization via the modular transformation \mathcal{T} . It is similar to the entanglement spectrum method [35] based on the wave function in the bulk. Here we directly use the edge density profile to calculate the momentum polarization similar to the finite DMRG method [42] and, of course, a larger system size could be reached by Monte Carlo method. Because of the bulk-edge correspondence, these results are intercomparable.

The rest of the paper is organized as follows. In Sec. II, we calculate the occupation numbers for several FQH states in cylinder geometry and revisit the exponents of the edge chiral boson theory (CBT). In Sec. III, we calculate topological quantities from edge dipole moment and momentum polarization. In Sec. IV, we obtain the TL exponent α from equal time Green's function and discuss the validity of the TL theory. The MR and 331 states are also considered. Section V gives the conclusions and discussions.

II. THE OCCUPATION NUMBER AND ITS SCALING BEHAVIORS

We first introduce the occupation number calculation by Metropolis Monte Carlo which was previously implemented in disk geometry [46–48]. The disk geometry in a symmetric gauge has unequally spaced orbits which evolves many more orbitals for the edge profile and induces slowing the

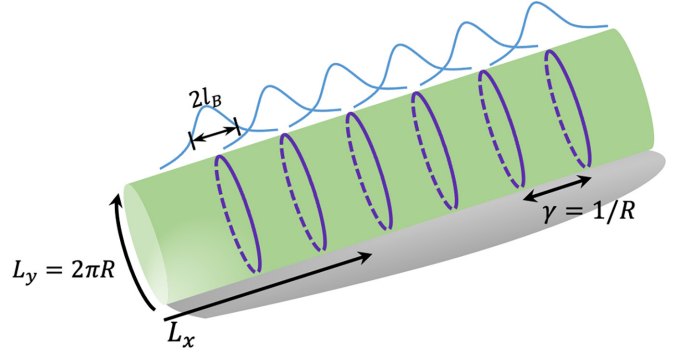


FIG. 1. The sketch map of cylinder model with L_x and L_y in two directions. $L_y = 2\pi R$ is the circumference of cylinder, and the reciprocal of the radius is defined as $\gamma = 1/R$.

convergence of the bulk density. In this paper, as shown in the sketch of Fig. 1, we use the cylinder geometry which has advantages that the space between adjacent Landau orbits is homogeneous and the length of the edge of the two ends is tunable by varying the aspect ratio L_x/L_y , while keeping the surface area invariant. The normalized N -electron Laughlin wave function $|\psi_{1/q}^c\rangle$ at filling $\nu = 1/q$ is [49,50]

$$|\psi_{1/q}^c\rangle = \frac{1}{\sqrt{N!}} \frac{1}{(2\pi\gamma^{-1}\sqrt{\pi})^{N/2}} \exp\left(-\frac{9}{2}\gamma^2 \sum_{j=0}^{N-1} j^2\right) \times \prod_{j<k} (e^{\gamma\mathbf{z}_j} - e^{\gamma\mathbf{z}_k})^q e^{-\frac{1}{2}\sum_{i=1}^N x_i^2} e^{-\sum_i \frac{q}{2}(N-1)\mathbf{z}_i}, \quad (1)$$

in which $\mathbf{z}_i = (x_i + iy_i)/l_B$ is the coordinate of the i th particle, l_B is the magnetic length $l_B = \sqrt{\hbar/eB}$ which we set to one, and the Landau orbital space $\gamma = 2\pi/L_y = 1/R$ where R is the radius of the cylinder. The last term is a global shift which lets the FQH state be symmetric around the center of cylinder at $x = 0$. The average occupation of the m th single-particle state is

$$\langle c_m^\dagger c_m \rangle_{1/q} = \frac{\langle \psi_{1/q}^c | c_m^\dagger c_m | \psi_{1/q}^c \rangle}{\langle \psi_{1/q}^c | \psi_{1/q}^c \rangle} = \int d^2z_1 d^2z_2 \rho_{1/q}(\mathbf{z}_1, \mathbf{z}_2) \phi_m^{c*}(\mathbf{z}_1) \phi_m^c(\mathbf{z}_2), \quad (2)$$

where $\rho_{1/q}$ is the one-particle density matrix [51] and $\phi_m^c(\mathbf{z}) = \frac{1}{\sqrt{\pi^{1/2}L_y}} e^{iky} e^{-(x-k)^2/2}$ is the wave package of the lowest Landau level in a Landau gauge with wave vector $k = \frac{2\pi m}{L_y}$. Now the y direction translation momentum quantum number m 's are symmetrically distributed in range $[-\frac{q(N-1)}{2}, \frac{q(N-1)}{2}]$. The one-particle density matrix is

$$\rho_{1/q}(\mathbf{z}_a, \mathbf{z}_b) = N \int d^2\mathbf{z}_2 \cdots \int d^2\mathbf{z}_N \psi_{1/q}^c(\mathbf{z}_a, \mathbf{z}_2 \cdots \mathbf{z}_N) \times \psi_{1/q}^{c*}(\mathbf{z}_b, \mathbf{z}_2 \cdots \mathbf{z}_N) / \int \prod_{i=1}^N d^2\mathbf{z}_i |\psi_{1/q}^c|^2. \quad (3)$$

Because ϕ_m^c and $|\psi_{1/q}^c\rangle$ conserve the translation momentum operator along y , the one-particle density matrix could be

written in second quantized form:

$$\rho_{1/q}(\mathbf{z}_a, \mathbf{z}_b) = \sum_m \langle c_m^\dagger c_m \rangle_{1/q} \phi_m^c(\mathbf{z}_a) \phi_m^{c*}(\mathbf{z}_b). \quad (4)$$

In the special case of $\mathbf{z}_a = x + iy$ and $\mathbf{z}_b = x + i(y + y_j)$, namely, \mathbf{z}_a and \mathbf{z}_b have the same x and a shift y_i in y :

$$\rho_{1/q}(\mathbf{z}, \mathbf{z} + iy_j) = \sum_k \langle c_k^\dagger c_k \rangle_{1/q} |\phi_k^c(\mathbf{z})|^2 e^{iky_j}. \quad (5)$$

Since $\langle c_k^\dagger c_k \rangle_{1/q}$ is nonzero over a contiguous, finite, and known range $k \in [-\frac{2\pi}{L_y} \frac{q(N-1)}{2}, \frac{2\pi}{L_y} \frac{q(N-1)}{2}]$, the summation over k can be restricted to this range without any uncertainty. Then the above relation could be explained as a discrete Fourier transformation from momentum space k to real space conjugate y . The inverse transformation has the following form:

$$\langle c_k^\dagger c_k \rangle_{1/q} |\phi_k^c(\mathbf{z})|^2 = \frac{1}{N_{\text{orb}}} \sum_{j=0}^{q(N-1)} e^{-iky_j} \rho_{1/q}(\mathbf{z}, \mathbf{z} + iy_j), \quad (6)$$

where $y_j = \frac{L_y}{N_{\text{orb}}} j$, and $N_{\text{orb}} = qN - q + 1$ is the number of orbits. Note that Eq. (6) is only true for $-\frac{q(N-1)}{2} \leq m \leq \frac{q(N-1)}{2}$. In principle, Eq. (6) is valid for any value of z , but practically the resulting uncertainty in the occupation number will be a minimum when r is near the maximum in $|\phi_k^c(\mathbf{z})|^2$, which occurs at $z \sim my_l_B$. We evaluate the occupation number by integrating Eq. (6) over \mathbf{z} to get

$$\langle c_k^\dagger c_k \rangle_{1/q} = \frac{1}{N_{\text{orb}}} \sum_{j=0}^{N_{\text{orb}}-1} e^{-iky_j} \rho_{1/q}(y_j), \quad (7)$$

where $\rho_j = \rho_{1/q}(y_j) = \int d^2z \rho_{1/q}(\mathbf{z}, \mathbf{z} + iy_j)$. Then the occupation at any k (within the appropriate range) can be found after evaluating ρ_j for all $j = 0, \dots, N_{\text{orb}} - 1$. From Eq. (3), we have

$$\rho_j = \frac{N \int \prod_{i=1}^N d^2z_i \psi_{1/q}^c(\mathbf{z}_1 - i\mathbf{y}_j, \dots, \mathbf{z}_N) \psi_{1/q}^{c*}(\mathbf{z}_1, \dots, \mathbf{z}_N)}{\int \prod_{i=1}^N d^2z_i |\psi_{1/q}^c|^2}. \quad (8)$$

Ignoring the normalization factor, Eq. (1) becomes

$$\psi_{1/q}^c(\mathbf{z}_1 - i\mathbf{y}_j, \mathbf{z}_2, \dots) = \psi_{1/q}^c(\mathbf{z}_1) Z_1(y_j, \mathbf{z}), \quad (9)$$

where

$$Z_b(y_j, \mathbf{z}) = \prod_{k \neq b} \frac{(e^{\gamma(z_b - iy_j)} - e^{\gamma z_k})^q}{(e^{\gamma z_b} - e^{\gamma z_k})^q} e^{i\gamma \frac{q(N-1)}{2} y_j}, \quad (10)$$

thus, we have

$$\rho_j = \frac{N \int \prod_{i=1}^N d^2z_i |\psi_{1/q}^c|^2 Z_1(y_j, \mathbf{z})}{\int \prod_{i=1}^N d^2z_i |\psi_{1/q}^c|^2}. \quad (11)$$

Finally, ρ_j can be expressed as

$$\rho_j = \frac{\int \prod_{i=1}^N d^2z_i |\psi_{1/q}^c|^2 \sum_{b=1}^N Z_b(y_j, \mathbf{z})}{\int \prod_{i=1}^N d^2z_i |\psi_{1/q}^c|^2}, \quad (12)$$

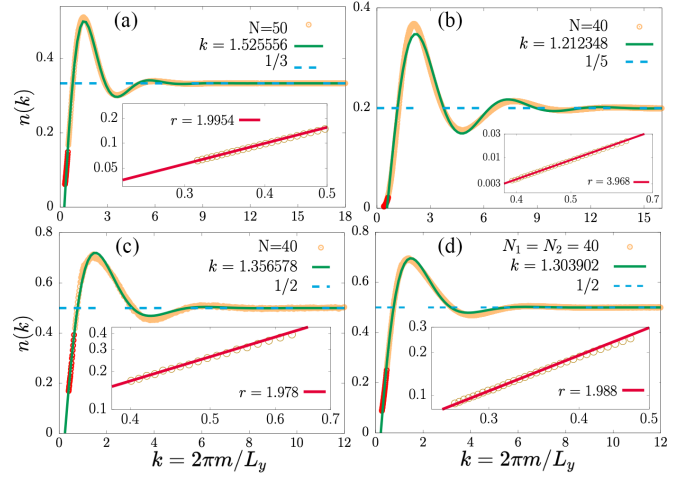


FIG. 2. Occupation numbers at the edge of (a) $\nu = 1/3$ state for 50 particles, (b) $\nu = 1/5$ state for 40 particles, (c) $\nu = 5/2$ MR state for 40 particles, and (d) 331 state for 80 particles (40 in each layer). The inset plots are the linear fit in logarithmic scale for the data near the Fermi point [labeled in red circles in $n(k)$]. The slopes are $r_{1/3} = 1.99541 \pm 0.008402$, $r_{1/3} = 1.9954(84)$, $r_{1/5} = 3.968(38)$, $r_{\text{MR}} = 1.978(34)$ and $r_{331} = 1.988(46)$, which are exactly the same as predicted in CBT. The results are rounded.

where we have symmetrized Z_b over all particle indices to increase the rate of convergence without loss of generality. The above expression can be evaluated through Metropolis sampling with high accuracy. We can then obtain the average occupation number of the $1/q$ Laughlin state on cylinder after going back to Eq. (7). In a similar scheme, we obtained the occupation numbers for other FQH states, such as the Moore-Read Pfaffian state and two-component Halperin 331 state. The technical details for these states are in Appendixes A and B.

With the occupation numbers for large systems, including $\nu = 1/3, 1/5$ Laughlin states, $\nu = 5/2$ Moore-Read, and Halperin 331 states, we verify the behavior of n_k near the edge by comparing to the CBT with high accuracy. The magnetoroton minimum could also be fitted in a large range, specifically for $1/5$ and 331 states, since the size of Hilbert space is extremely large in exact diagonalization. The bulk density is difficult to reach the uniform density $\rho = \nu/2\pi l_B^2$ and thus many of the physical quantities are obscured by finite-size effects. Figure 2 shows half of the occupation numbers for these states due to central symmetry. The occupation numbers are plotted as a function of the wave vector $k = \frac{2\pi m}{L_y}$ rather than the orbital index m . By properly choosing the Fermi points [35] to assure there are N/ν orbitals between two Fermi points, i.e., the momentum of the first nonvanishing occupation number is $m_0 = 3/2$ for $\nu = 1/3, 5/2$, and 331 states and $m_0 = 5/2$ for $\nu = 1/5$ state, the data for different circumferences L_y (the L_y takes value in the range (a) $[19l_B, 30l_B]$, (b) $[25l_B, 40l_B]$, (c) $[15l_B, 23l_B]$, and (d) $[20l_B, 35l_B]$ to make sure the two edges are well separated) collapses into a perfectly smooth curve which manifests the universality of the FQH edge, since we now have much more data near Fermi points and no breakpoints as compared to the results from Jack polynomials [35]. The $n(k)$ near the edge clearly

demonstrates that the FQH edge is described by the CBT with $n_k \propto k^r$ in which $r = \nu^{-1} - 1$ for Laughlin states. Thus, we take the linear fit of $\ln n(k)$ versus $\ln k$ with the first nonvanishing occupation number of different L_y . For the four FQH states we considered, the CBT predicts their exponents to be $r = 2, 4, 2, 2$, respectively. Our simulation gives these fitting values as $r_{1/3} = 1.9954 \pm 0.0084$, $r_{1/5} = 3.968 \pm 0.038$, $r_{\text{MR}} = 1.978 \pm 0.034$, and $r_{331} = 1.988 \pm 0.046$ as shown in the insets of each panel in Fig. 2. They are exactly the same as the expected value within the statistical error.

On the other hand, as in Ref. [34], we fit the oscillations of the occupation numbers by $f_\nu(x) = c_\nu \exp(-x/\epsilon_\nu) \cos(k_\nu x + \theta_\nu) + \nu$. It was claimed that k_ν is in good agreement with the wave number of the bulk magnetoroton minimum and ϵ_ν is proportional to the bulk excitation gap. Density oscillation at the edge reflecting bulk excitation is a good example of bulk-edge correspondence in the topological ordered phase. From our simulations of model wave functions, the fitting parameters are $\epsilon_{1/3} = 1.357$, $k_{1/3} = 1.526$; $\epsilon_{1/5} = 2.415$, $k_{1/5} = 1.212$, $\epsilon_{5/2} = 1.185$, $k_{5/2} = 1.357$ and $\epsilon_{331} = 1.08$, $k_{331} = 1.304$, respectively. Here we should note that our results are for model wave functions that correspond to the eigenstates of the model Hamiltonian, such as a V_1 Haldane pseudopotential Hamiltonian for the $\nu = 1/3$ Laughlin state. Realistic Coulomb interaction naturally gives different results, especially energies. Compared to the result of DMRG with Coulomb interaction [34], the $k_{1/3}$ is quite close and $\epsilon_{1/3}$ is very different, as expected, since the wave function is quite close and the energy should be different. Therefore, we expect that the magnetoroton minimums for the other three FQH states (1/5, MR, and 331) in Coulomb Hamiltonian are almost the same as the k_ν we obtained.

III. TOPOLOGICAL QUANTITIES FROM MOMENTUM POLARIZATION

It is known that quasihole mutual exchange in FQH liquids contains rich information about its topological order. Suppose we have a quasihole on each edge of the cylinder—rotation along the direction of y will not give any information because of the rotation symmetry of this manifold. However, if one can rotate half of the cylinder (subsystem A) and keep the other half (subsystem B) unchanged, the many-body wave function will have a phase containing the information of the quasihole in subsystem A . This phase is called momentum polarization [39], which contains important topological quantities such as Hall viscosity [38], guiding-center spin, central charge, and topological spin (conformal dimension) of quasihole excitation. Momentum polarization has previously been studied using the entanglement entropy in cylinder geometry [39] and modular transformation in torus geometry [40,41]. It could also be studied in the entanglement spectrum at the bipartite boundary in the bulk and the intrinsic dipole moment from the density profile on the edge [35,40].

Here we firstly employ the occupation numbers to calculate momentum polarization. It can be acquired by

$$\langle \Delta M_A \rangle = \sum_{m \in A} m(n_m) - M_A^0 \quad (13)$$

where M_A^0 just depends on the root occupation number, such as 1001001001..., 1000010000100001..., 1100110011.... Theoretically, momentum polarization contains three leading terms as follows:

$$\langle \Delta M_A \rangle = \frac{\eta_H}{2\pi\hbar} L_y^2 - h_\alpha + \frac{\gamma}{24}, \quad (14)$$

where the first term is derived from the contribution of the guiding-center Hall viscosity. The second term $h_\alpha = M_A^0 - \bar{M}_A$ is called topological spin [39,41] or conformal spin of elementary excitations that corresponds to the quasihole sector α and depends on the position of the bipartition in the occupation space. It can be calculated for different model FQH states by using the root configuration pattern in the Jack polynomial description or the conformal field correlator of quasihole operators as shown in Appendix D. The third leading term $\gamma = \tilde{c} - \nu$ is the difference between the (signed) conformal anomaly ($\tilde{c} = c - \bar{c}$) and the chiral charge anomaly (filling factor) ν , which are the two fundamental quantum anomalies of FQH fluids. The theoretical values are as follows: $c = 1$ for Laughlin states, $c = 3/2$ for the 5/2 Moore-Read state, and $c = 2$ for bilayer 331 state, and all chiral states have $\bar{c} = 0$. Notice that γ vanishes in IQH states, which are topologically trivial.

In the case of FQH fluid, the edge density deviates from the uniform density $\nu/2\pi l_B^2$ due to the electron-electron correlation. This nonuniform occupation distribution gives a quantized dipole moment p_x , which is related to the guiding-center Hall viscosity (the expected value of area-preserving deformation generators) [35,40]. The essential physics here is the intrinsic dipole momentum coupling with the gradient of the electric field from Coulomb interaction and confining potential. This coupling results in an electric force that is balanced by the guiding center Hall viscosity η_H . Moreover, the guiding center Hall viscosity was found to have a relation to a topological quantity named the guiding-center spin. $\eta_H^{ab} = -\frac{\hbar}{4\pi l_B^2} \frac{s}{q} g^{ab}$, where g^{ab} is the guiding-center metric in Haldane's geometric description of FQH liquid [52] and the guiding-center spin s coupled with curvature gives the topological shift on the sphere. Finally, we have the relationship

$$\eta_H = -\frac{p_x}{L_y} B = \frac{\hbar}{4\pi l_B^2} \frac{-s}{q}, \quad (15)$$

where B is the strength of magnetic field and q is the flux quantum number attached by a composite boson that is made of p particles with q flux quanta for $\nu = p/q$. After a simple substitution, we have

$$\langle \Delta M_A \rangle = -\frac{1}{2} \left(\frac{L_y}{2\pi l_B} \right)^2 \frac{s}{q} - h_\alpha + \frac{c - \nu}{24}. \quad (16)$$

The edge dipole moment per length could be calculated from the occupation numbers as follows:

$$\frac{p_x(k)}{L_y} = -\frac{e}{2\pi} \int_0^k dk' k' l_B^2 [n(k') - \nu], \quad (17)$$

and for finite L_y , compare to Eq. (16), the integration is approximated by the sum with corrections:

$$\frac{p_x(k)}{L_y} = -\frac{2\pi l_B^2 e}{L_y^2} \left(\sum_{m'} [n(m') - \nu] m' + h_\alpha - \frac{c - \nu}{24} \right). \quad (18)$$

Here we should note that the origin paper of Eq. (37) in Ref. [35] does not have correction terms and the difference is also discussed in detail in a recent work [40]. It is due to the equivalence of intrinsic dipole moment and momentum polarization, which can be considered as the same topological quantity. On the other hand, we point out that this may also be the reason why Figs. 16–20 in Ref. [35] are less convergent. A slight shift between theoretical and numerical values is clearly observed there, which is clearly not a finite-size effect. The quantities s , h_α , c contain very rich information. Guiding center spin s is related to the nondissipative response of metric perturbation [42]. Topological spin h_α and central charge c are elements of the modular- T matrix, which is the unitary transformation of the ground-state manifold under modular transformation [43].

In our simulation process, we use a self-consistent test method to determine these topological quantities, namely, we set the other quantities at their respective theoretical values when calculating one of them. For example, while calculating the central charge c , the guiding center spin and topological spin are predetermined by their CFT values and thus

$$c = 24(\Delta M_A) + 24 \frac{L_y^2}{8\pi^2} \left(-\frac{1}{3} \right) + 24h_\alpha + \frac{1}{3}. \quad (19)$$

For the $\nu = 1/3$ Laughlin state, the results of the topological spin strongly depend on how many quasiparticles the subsystem has. This could be adjusted by shifting the bipartite position in the root configuration of the Jack description [53,54]. Basically, there are three topological sectors for the $1/3$ Laughlin state with root $010010 \dots 010010$. One is the equal bipartition with $\dots 10|01 \dots$ named vacuum cut, in which case the subsystem of N_A particles exactly occupies $N_A/\nu = 3N_A$ orbitals and thus no quasiparticle (quasihole) excitation. If one more (less) orbit is allocated to the subsystem, such as $\dots 100|1 \dots (\dots 1|001 \dots)$, a quasihole (quasiparticle) is created in the left subsystem. The different bipartitions and their corresponding topological spins in other FQH states are discussed in Appendix D. Finally, for a specific system with a fixed number of electrons, we calculated these topological quantities by varying the aspect ratio of the cylinder, or changing the L_y to keep the area invariant. Therefore, each L_y gives a set of results as shown in all of the following results.

Combining Eqs. (15) and (18), considering the contribution of central charge c and topological spin h_α [39] to the guiding-center spin, and discretizing the momentum, we have

$$-\frac{s}{q} = \frac{8\pi^2}{L_y^2} \left(\sum_{m_1} (n(m_1) - \nu) m_1 + h_\alpha - \frac{c - \nu}{24} \right). \quad (20)$$

Before calculating the guiding-center spin, we need to validate the Luttinger's sum rule [55], i.e., charge neutral conditions

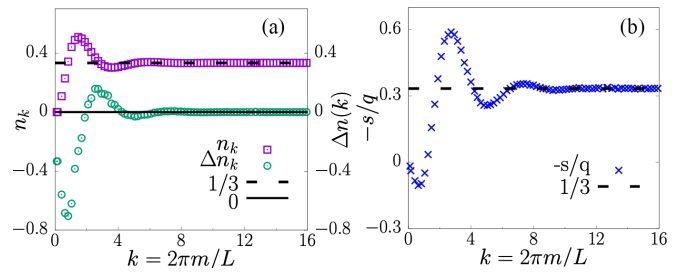


FIG. 3. (a) $\Delta n(k)$ and $-s/q$ in half of the cylinder for $1/3$ Laughlin state with 50 particles. The $\Delta n(k)$ converges to 0 and verifies the electrical neutrality condition and convergence of the simulation. (b) The $-s/q$ converges perfectly with the expected value and thus $s = -1$.

$\sum_{m_1} [n(m_1) - \nu] = 0$. Our numerical results are shown in Figs. 3–6. First, we check Luttinger's sum rule. The difference Δn_k between the occupation number and the uniform occupation ν converges to zero. Then, the $-s/q$ converges to $1/3, 2/5, 1/2, 1/2$, respectively, giving us the guiding-center spin for the $1/3, 1/5$ Laughlin state, $5/2$ MR state, and 331 state as $s = -1, -2, -2, -2$, respectively.

Let us go back to Eq. (16) to calculate the other topological quantities. We extract these topological quantities numerically for different FQH states. The results are shown in Figs. 7–9. First, we observe that Monte Carlo simulations of large systems actually give us much more accurate topological quantities of FQH states. These values are in good agreement with the theoretical predictions of the CFT. For example, we get $c = 1, 1, 3/2, 2, s = -1, -2, -2, -2$ for the $1/3, 1/5$ Laughlin states, Moore-Read state, and 331 state, respectively. As for topological spin, all theoretical predictions are presented in Appendix D. Compared with the previous study by the matrix product state with a low truncation level [35], the accuracy of our method is prominent and the computational cost is effective. Especially for the $1/5$ Laughlin state, it is found that the convergence of these topological quantities is very slow compared to the $1/3$ Laughlin state. For example, Fig. 7(c) shows that the central charge has significantly larger fluctuations than that in Fig. 7(a). The slow convergence of $1/5$ is clearly shown in the range of edge density fluctuations in Fig. 4.

From Figs. 5, 6, and 8, we can see that except for the central charge c , all other topological quantities are the same for the Moore-Read state and 331 state. It is known that their $e/4$ quasihole excitations are very different in anyonic statistics.

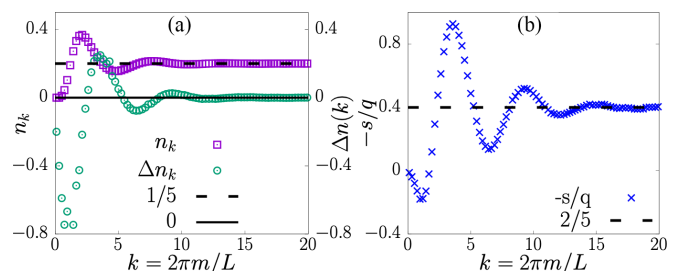


FIG. 4. Same as Fig. 3 for $1/5$ with 40 particles. The guiding center spin converges to $s = -2$.

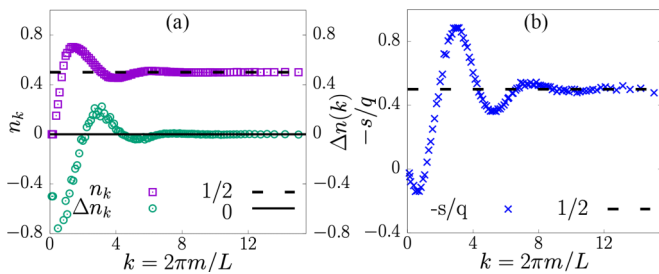


FIG. 5. Same as Fig. 3 for MR state with 40 particles. The guiding center spin converges to $s = -2$.

The $e/4$ quasihole in the Moore-Read state is non-Abelian because it contains a Majorana mode and that in the 331 state is trivial Abelian. Here we model these quasiholes at the edge of the cylinder in Monte Carlo (details are shown in Appendix E) and calculate their topological quantities as shown in Fig. 9. From this, we find that the central charge and guiding-center spin are the same as the ground state. However, for topological spin of the $e/4$ quasihole, numerical results show that $h_\alpha = 1/8$ for the Moore-Read state and $h_\alpha = 3/16$ for the 331 state. These values are in good agreement with their theoretical predictions, as shown in Appendix D, which demonstrates their different topological properties.

IV. EDGE GREEN'S FUNCTION

Owing to the existence of gapless edge states in FQH liquids with open boundaries, current exists between two contacts connected by an edge channel, as electrons can be injected into or removed from the FQH edge with costing zero energy. The standard theory for FQH edge physics is χ LL theory [3,12]. The theory predicts that a FQH droplet exhibits a power-law behavior in the electric current-voltage characteristics ($I \propto V^\alpha$) when electrons tunnel through a barrier into the FQH edge from a Fermi liquid [3,12,17,20]. Generally, α is also a topological quantity that is related to the topological order of the FQH liquid and immune to perturbations. For the celebrated $\nu = 1/3$ Laughlin state, the χ LL theory predicts a tunneling exponent $\alpha = 3$ although it is controversial in realistic systems, as we mentioned in the Introduction. The α measured in experiments is sample dependent with a value mostly smaller than 3 [17–20]. One of the possible causes of this discrepancy is the existence of counterpropagating edge modes, which result from edge reconstruction [23–27]. The

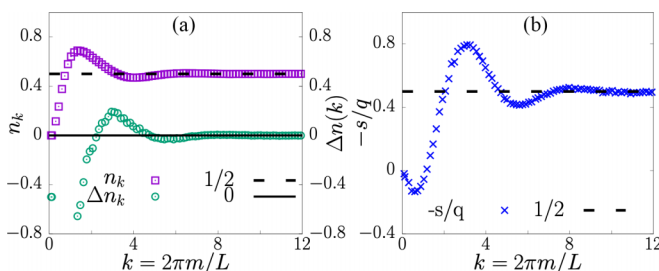


FIG. 6. Same as Fig. 3 for 331 state with 80 particles. The guiding center spin converges to $s = -2$.

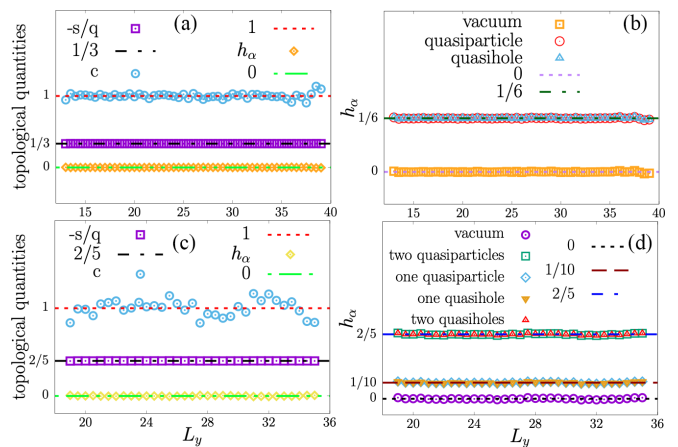


FIG. 7. Topological quantities for $\nu = 1/3$ and $\nu = 1/5$ Laughlin states. In (a) and (c), we present the results of $-s/q$, c , and h_α in the vacuum cut. (b) and (d) show h_α for different bipartitions. The corresponding theoretical results are marked by horizontal dash lines.

χ LL theory [14,15] also predicts the $\alpha = 5$ for $1/5$ Laughlin state and $\alpha = 3$ for both the Moore-Read and 331 states. The relevant experimental and theoretical values for the Laughlin states are in Refs. [4,18,56,57].

Numerically, we can obtain α by calculating the electron edge Green's function which is the electron propagator along the edge of the FQH droplet. The scaling behavior of the edge Green's function has been studied in disk geometry [22–24]. As previously claimed, the disk geometry has inhomogeneous Landau orbital space and thus the edge density profile is always incomplete in small system sizes. Another problem is that the edge distance is limited by the circumference of disk and the scaling behavior suffers from strong finite-size effects. Monte Carlo simulation in cylinder geometry could overcome these weaknesses because the length scale of the edge could be tuned by aspect ratio. In cylinder geometry, the

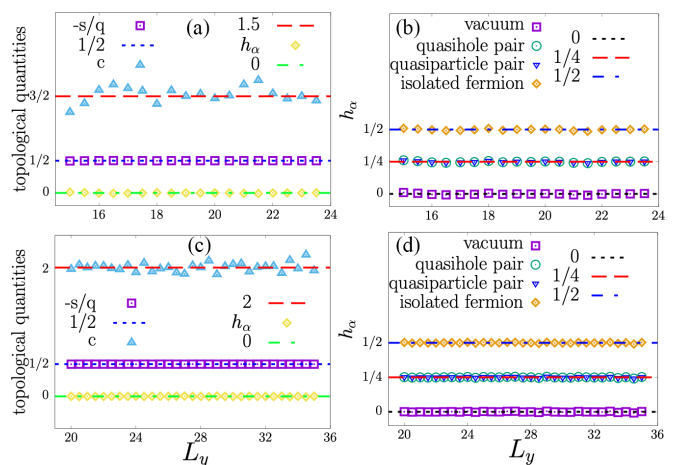


FIG. 8. Same as Fig. 7. Topological quantities for MR and 331 states. Here the quasihole/quasiparticle is $e/2$ charged because one orbit is shifted in the occupation number configuration.

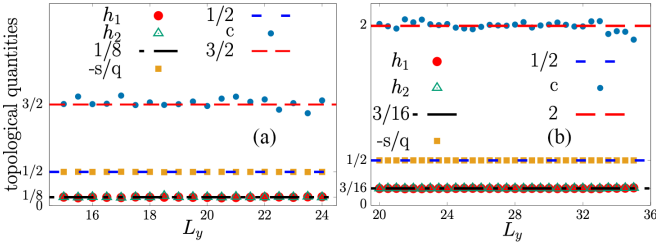


FIG. 9. Topological quantities for (a) Moore-Read state and (b) 331 state with $e/4$ quasihole excitation at the edge.

edge Green's function can be defined as

$$G_{\text{edge}}(|\vec{z} - \vec{z}'|) = \frac{N \int \prod_{j=1}^{N-1} d^2 z_j \psi^*(\vec{z}, \{\vec{z}_j\}) \psi(\vec{z}', \{\vec{z}_j\})}{\int \prod_{k=1}^N d^2 z_k \psi^*(\{\vec{z}_k\}) \psi(\{\vec{z}_k\})}, \quad (21)$$

where \vec{z} and \vec{z}' are on the same edge of the cylinder, and they have the same value of x coordinates. At the limit of large distance ($|\vec{z} - \vec{z}'| \gg 1$), the Green's function behaves as

$$G_{\text{edge}}(|\vec{z} - \vec{z}'|) \sim |\vec{z} - \vec{z}'|^{-\alpha}. \quad (22)$$

From Appendix C, the equal-time edge Green's function on the cylinder can be written as

$$G_{\text{edge}}\left(\left|\frac{2}{\gamma} \sin\left(\frac{Y\gamma}{2}\right)\right|\right) = \sum_k \frac{1}{\pi^{1/2} L_y} e^{-iky} e^{-(X-k)^2} n_k. \quad (23)$$

The chord distance is $|\frac{2}{\gamma} \sin(\frac{Y\gamma}{2})|$ where $Y = |y_1 - y_2|$ is the arc length between \vec{z} and \vec{z}' on the surface of cylinder and $\gamma = 2\pi/L_y = 1/R$ is the inverse of the radius or space between two continuous Landau orbits.

For an N -particle FQH liquid at filling ν , the number of Landau orbits is N/ν and thus the length of the cylinder is $\frac{2\pi N}{\nu L_y} = N\gamma/\nu$. Two edges locate at $\pm N\gamma/2\nu$. As shown in Figs. 10(a) and 10(b), we plot half the density profile for the four states. Here we set the x coordinate to $\tilde{X} = X - N\gamma/2\nu$

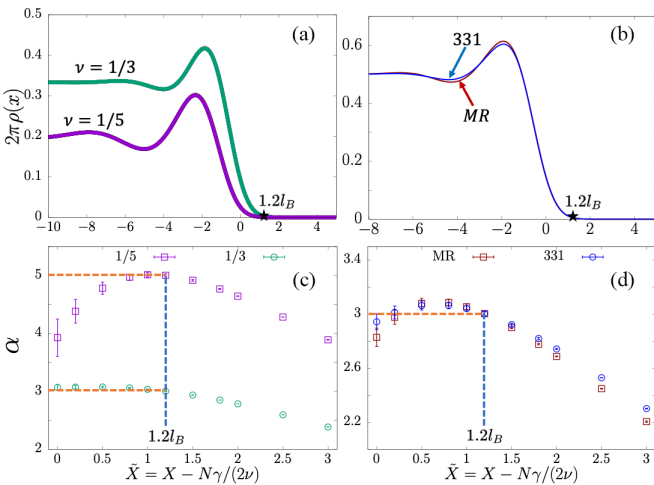


FIG. 10. The density profiles (a), (b) and scaling exponents of the edge Green's functions at different \tilde{X} (c), (d). Here the x -axis is set to $\tilde{X} = X - N\gamma/(2\nu)$, where $N\gamma/(2\nu)$ is the physical edge on the right. The theoretical predictions of the respective FQH states are marked as horizontal dashed lines.

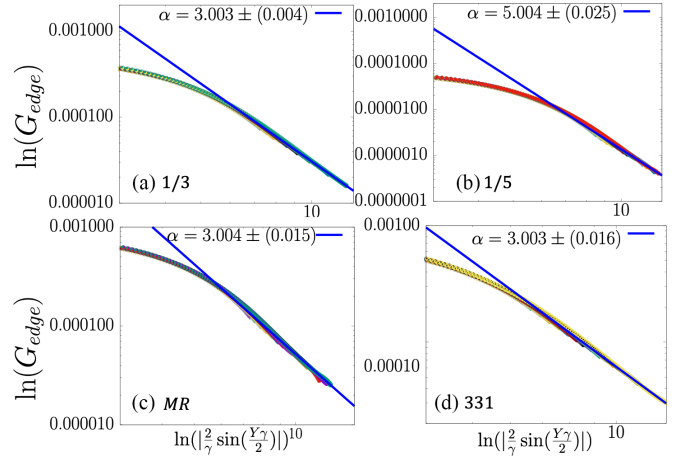


FIG. 11. The edge Green's function at $\tilde{X} = 1.2l_B$ for (a) $1/3$ Laughlin state, (b) $1/5$ Laughlin state, (c) MR state, and (d) 331 state.

and then the edge on the right is positioned at $\tilde{X} = 0$. First, as we mentioned earlier, the $1/5$ state has a deeper density oscillation than that of the $1/3$ state. Comparing the Moore-Read state and 331 state with the same electron number and L_y , the bulk density is the same since both are candidates for the $\nu = 5/2$ FQH state. However, it is shown that the edge density has certain differences that demonstrates they belong to different topological phases or have different topological quantities such as the central charge as described in the previous section. For the Green's function along the edge, we fix the x position and calculate Eq. (21) in the y direction. Because the density profile always has a tail near the edge, we sweep the position of \tilde{X} around $\tilde{X} = 0$. For each \tilde{X} , we calculate the Green's function and extrapolate the exponent α by the data of the large distance. The results are shown in Figs. 10(c) and 10(d). Overall, we find that α has a dependence on \tilde{X} . The interesting thing is that α for all four states reach their respective theoretical values around $\tilde{X} \simeq 1.2l_B$, which is indicated by a star in Figs. 10(a) and 10(b). When $\tilde{X} > 1.2l_B$, we find α always decays and becomes smaller than the theoretical value. We understand this result as that the edge of the FQH liquid always has a width in the order of one magnetic length l_B . The Luttinger liquid exponent has its exact value at the tail of the realistic edge where the electron density is close to zero, as shown in Figs. 10(a) and 10(b). This is acceptable because only the electrons at the tail of the edge are on the Fermi points and have gapless excitation. Electrons that are away from Fermi points require finite energy to excite and therefore cannot be strictly described as gapless edge excitation, or χ LL theory.

At $\tilde{X} = 1.2l_B$, we show the Green's function as a function of chord distance in a logarithmic plot in Fig. 11. Similar to the density profile, the edge Green's function for different L_y (aspect ratio) collapses into a curve with a small finite-size fluctuation. The α shown in the figure is obtained by fitting the data for large chord distances. The Moore-Read state and the 331 state share the same α , which illustrates electron tunneling, such as in the strong tunneling limit of the QPC experiment, and cannot distinguish the two unequal states. However, since their $e/4$ quasiholes have different topological

quantities as calculated in the momentum polarization, we expect the quasihole tunneling, such as in the weak tunneling limit of QPC, could give their distinctions.

V. SUMMARIES AND DISCUSSIONS

In this paper, we have applied a Metropolis Monte Carlo method to calculate the electron occupation numbers of the Landau orbits for wave functions of the FQH model in cylinder geometry. We consider large systems with more than 40 electrons of $\nu = 1/3, 1/5$ Laughlin states and two candidates for $\nu = 5/2$ FQH states, namely, the Moore-Read Pfaffian state and Halperin bilayer 331 state. With smooth data near the edge, the full density profiles of the edge states are obtained and the CBT of the FQH edge has been verified with high accuracy. As a first check of the effectiveness of this method, we numerically determine the topological quantities using the dipole moment and momentum polarization calculations. The guiding-center spin, central charge, and topological spin of the quasihole all converge exactly to their respective theoretical values. Notably, due to the non-Abelian nature of MR $e/4$ quasihole excitation, its topological spin is very different from its Abelian counterpart in the 331 state. We model the $e/4$ quasihole excitation in both states and identify their topological spins, which are consistent with CFT predictions. With the occupation numbers of large systems, another quantity we recalculated is the non-Fermi liquid behavior of the electron Green's function along the edge. Sweeping the locations, we find that only electrons near the physical boundary have the theoretically predicted α . Therefore, we conclude that the χ LL theory is an idealized description of the boundary of the FQH liquid. This could be another possible mechanism where α is not quantized and the sample is dependent on realistic experiments even in the absence of edge reconstruction. This method could be easily generalized to other FQH states or the interface between different FQH states.

ACKNOWLEDGMENTS

Z.-X. Hu thanks H.-H. Tu for helping us to explain the 331 state in CFT description. Y.Y. thanks C.-X. Jiang for numerical skill discussions. The Pfaffian polynomial calculation was implemented by using the algorithm in Ref. [58]. This work was supported by National Natural Science Foundation of China Grants No. 11974064 and No. 12147102, the Chongqing Research Program of Basic Research and Frontier Technology Grant No. cstc2021jcyjmsxmX0081, Chongqing Talents: Exceptional Young Talents Project No. cstc2021ycjhbgzxm0147, and the Fundamental Research Funds for the Central Universities Grant No. 2020CDJQY-Z003.

APPENDIX A: MOORE-READ STATE

The Moore-Read Pfaffian model wave function in cylinder geometry could be written as

$$\begin{aligned} |\psi_{5/2}^c\rangle &= \text{Pf}[M(e^{\gamma Z})] \prod_{j < k} [\exp(\gamma \mathbf{z}_j) - \exp(\gamma \mathbf{z}_k)]^2 \\ &\times e^{-\frac{1}{2} \sum_{i=1}^N x_i^2} e^{-\sum_i \frac{(2N-3)\gamma}{2} \mathbf{z}_i}, \end{aligned} \quad (\text{A1})$$

where $\text{Pf}[M(e^{\gamma Z})]$ is the Pfaffian polynomial of the antisymmetric matrix $M(e^{\gamma Z})$. For four particles, it is

$$\begin{aligned} \text{Pf}[M(e^{\gamma Z})] &= \frac{1}{\exp(\gamma \mathbf{z}_1) - \exp(\gamma \mathbf{z}_2)} \frac{1}{\exp(\gamma \mathbf{z}_3) - \exp(\gamma \mathbf{z}_4)} \\ &- \frac{1}{\exp(\gamma \mathbf{z}_1) - \exp(\gamma \mathbf{z}_3)} \frac{1}{\exp(\gamma \mathbf{z}_2) - \exp(\gamma \mathbf{z}_4)} \\ &+ \frac{1}{\exp(\gamma \mathbf{z}_1) - \exp(\gamma \mathbf{z}_4)} \frac{1}{\exp(\gamma \mathbf{z}_2) - \exp(\gamma \mathbf{z}_3)}. \end{aligned} \quad (\text{A2})$$

In the Metropolis algorithm, we just need $|\text{Pf}(M(e^{\gamma Z}))|^2 = \det(M(e^{\gamma Z}))$. Using the same calculation method as the $1/q$ Laughlin state, we have

$$\rho_j = \frac{\int \prod_{i=1}^N d^2 z_i |\psi_{5/2}^c|^2 \sum_{b=1}^N Z_b(y_j, \mathbf{z})}{\int \prod_{i=1}^N d^2 z_i |\psi_{5/2}^c|^2}, \quad (\text{A3})$$

where

$$\begin{aligned} Z_b(y_j, \mathbf{z}) &= \prod_{k \neq b} \frac{(e^{\gamma(\mathbf{z}_b - i y_j)} - e^{\gamma \mathbf{z}_k})^2}{(e^{\gamma \mathbf{z}_b} - e^{\gamma \mathbf{z}_k})^2} \\ &\times e^{i\gamma(N-3/2)y_j} \frac{\text{Pf}[M(e^{\gamma R(\mathbf{z}_b \rightarrow \mathbf{z}_b - i y_j)})]}{\text{Pf}[M(e^{\gamma Z})]}, \end{aligned} \quad (\text{A4})$$

where $y_j = \frac{L_y}{N_{orb}} j$ with $j = 0 \cdots 2N - 3$ and k is from $-\frac{2\pi}{L_y} \frac{2N-3}{2}$ to $\frac{2\pi}{L_y} \frac{2N-3}{2}$. Similarly, we can obtain the average occupation number of the $5/2$ MR state on the cylinder by Metropolis sampling. We use the algorithm of Ref. [58] to implement the Pfaffian polynomial.

APPENDIX B: HALPERIN 331 STATE

For the bilayer Halperin 331 state on the cylinder, we assume that there are $N_1(N_2)$ electrons in the upper (lower) layer. The unnormalized wave function is

$$\begin{aligned} |\psi_{331}^c\rangle &= \prod_{i < j, i, j \in N_1} (\exp(\gamma \mathbf{z}_i) - \exp(\gamma \mathbf{z}_j))^3 \\ &\times \prod_{k < l, k, l \in N_2} (\exp(\gamma \mathbf{z}_k) - \exp(\gamma \mathbf{z}_l))^3 \\ &\times \prod_{i \in N_1, k \in N_2} (\exp(\gamma \mathbf{z}_i) - \exp(\gamma \mathbf{z}_k)) \\ &\times e^{-\frac{1}{2} \sum_{i=1}^N x_i^2} e^{-\sum_{i \in N_1} \frac{\gamma}{2} (4N_1 - 3) \mathbf{z}_i} e^{-\sum_{i \in N_2} \frac{\gamma}{2} (4N_2 - 3) \mathbf{z}_i}, \end{aligned} \quad (\text{B1})$$

where $N = N_1 + N_2$ is the total number of electrons. The total momentum is $\frac{3N_1(N_1-1)}{2} + \frac{3N_2(N_2-1)}{2} + N_1 N_2$. When $N_1 = N_2$, the total momentum is $M_{\text{tot}} = \frac{N(2N-3)}{2}$, which is the same as that of the Moore-Read state. Each layer has filling $1/4$. Similarly, we have

$$\rho_j = \frac{\int \prod_{i=1}^N d^2 z_i |\psi_{331}^c|^2 \sum_{b=1}^N Z_b(y_j, \mathbf{z})}{\int \prod_{i=1}^N d^2 z_i |\psi_{331}^c|^2}, \quad (\text{B2})$$

where

$$Z_b(y_j, \mathbf{z}) = \begin{cases} \prod_{k \neq b, k \in N_1} \frac{(e^{\gamma(z_b - iy_j)} - e^{\gamma z_k})^3}{(e^{\gamma z_b} - e^{\gamma z_k})^3} \prod_{k \in N_2} \frac{e^{\gamma(z_b - iy_j)} - e^{\gamma z_k}}{e^{\gamma z_b} - e^{\gamma z_k}} e^{i\gamma \frac{4N_1 - 3}{2} y_j}, & \text{if } z_b \in N_1 \\ \prod_{k \neq b, k \in N_2} \frac{(e^{\gamma(z_b - iy_j)} - e^{\gamma z_k})^3}{(e^{\gamma z_b} - e^{\gamma z_k})^3} \prod_{k \in N_1} \frac{e^{\gamma z_k} - e^{\gamma(z_b - iy_j)}}{e^{\gamma z_k} - e^{\gamma z_b}} e^{i\gamma \frac{4N_2 - 3}{2} y_j}, & \text{if } z_b \in N_2 \end{cases} \quad (\text{B3})$$

and $y_j = \frac{L_y}{N_{orb}} j$.

APPENDIX C: THE EDGE GREEN'S FUNCTION ON CYLINDER

Since the single-particle wave function is $\phi_k(z) = \frac{1}{\sqrt{\pi^{1/2} L_y}} e^{iky} e^{-(x-k)^2/2}$, the edge Green's function can be transferred to

$$\langle \phi^\dagger(\vec{z}_1) \phi(\vec{z}_2) \rangle = \sum_k \frac{1}{\pi^{1/2} L_y} e^{ik(y_2 - y_1)} \times e^{-(x_1 - k)^2/2} e^{-(x_2 - k)^2/2} \langle a_k^\dagger a_k \rangle. \quad (\text{C1})$$

The coordinates \vec{z}_1 and \vec{z}_2 are selected with the same position $x_1 = x_2 = X$ near the edge and have a shift in the y direction $Y = y_1 - y_2$, so the chord distance could be expressed as $|\frac{2}{\gamma} \sin(\frac{\gamma Y}{2})|$. Finally, the edge Green's function on the cylinder could be calculated by occupation numbers as

$$\langle \phi^\dagger(\vec{z}_1) \phi(\vec{z}_2) \rangle = \sum_k \frac{1}{\pi^{1/2} L_y} e^{-ikY} e^{-(X-k)^2} n_k. \quad (\text{C2})$$

APPENDIX D: TOPOLOGICAL SPIN

The topological spin h_α could be calculated from the root configuration in the occupation space as

$$h_\alpha = M_A^0 - \bar{M}_A. \quad (\text{D1})$$

The subscript α represents different topological sectors and depends on the location of the bipartition for subsystem A . $\bar{M}_A = -\frac{1}{2} \nu m_F^2$ is the total momentum for subsystem A with uniform occupation density ν , where m_F is the orbital number in A .

Taking the four-particle system as an example, for the $1/3$ Laughlin state, there are three topological sectors, vacuum cut sector $010010|010010$, quasiparticle cut sector $01001|0010010$, and quasihole cut sector $0100100|10010$. So, we have

$$\begin{aligned} 010010|010010 & h_\alpha = 0, \\ 01001|0010010 & h_\alpha = 1/6, \\ 0100100|10010 & h_\alpha = 1/6, \end{aligned} \quad (\text{D2})$$

where we only consider subsystem A on the left. The first momentum near the cut is $-1/2$. For example, for the quasiparticle cut sector, $M_A^0 = -\frac{1+7}{2} = -4$ and $\bar{M}_A = \frac{1}{3}(-\frac{1+3+5+7+9}{2}) = -\frac{25}{6}$, so $h_\alpha = -4 + \frac{25}{6} = \frac{1}{6}$.

For the $1/5$ Laughlin state, there are five topological sectors: vacuum cut $0010000100|0010000100$, two-quasiparticle cut $00100001|000010000100$, one-quasiparticle cut $001000010|00010000100$, one-quasihole

cut $00100001000|010000100$, and two quasihole cut $001000010000|10000100$. So, we have

$$\begin{aligned} 0010000100|0010000100 & h_\alpha = 0, \\ 00100001|000010000100 & h_\alpha = 2/5, \\ 001000010|00010000100 & h_\alpha = 1/10, \\ 00100001000|010000100 & h_\alpha = 1/10, \\ 001000010000|10000100 & h_\alpha = 2/5, \end{aligned} \quad (\text{D3})$$

Then, for the MR state, there are four topological sectors: vacuum cut $0110|0110$, isolated fermion cut $01|100110$, $e/2$ quasiparticle cut $011|00110$, and $e/2$ quasihole cut $01100|110$. We have

$$\begin{aligned} 0110|0110 & h_\alpha = 0, \\ 01|100110 & h_\alpha = 1/2, \\ 011|00110 & h_\alpha = 1/4, \\ 01100|110 & h_\alpha = 1/4. \end{aligned} \quad (\text{D4})$$

Since the $e/2$ quasihole/quasiparticle is just one more/less flux attached by electrons and both are Abelian, we assume that the $e/2$ excitation in the 331 state has the same properties as that in MR. This has been verified in the calculation of topological spins as shown in Fig. 8.

For $e/4$ excitation, the MR state and 331 state are distinct. Here we consider that each of the edges has a $e/4$ quasihole. Then the root configuration is $\dots 010101010 \dots$. In this case, there are two topological sectors: $\bar{0}101|0101\bar{0}$ and $\bar{0}1010|101\bar{0}$. we have

$$\begin{aligned} \bar{0}101|0101\bar{0} & h_\alpha = 1/8, \\ \bar{0}1010|101\bar{0} & h_\alpha = 1/8. \end{aligned} \quad (\text{D5})$$

For the quasihole MR state, since the total number of orbits is odd, the Fermi points are on top of the first orbit, which is labeled $\bar{0}$. It means that only half of this orbit belongs to the subsystem. For example, we consider the first sector of quasihole MR state, $M_A^0 = -\frac{1+5}{2} = -3$, and $\bar{M}_A = \frac{1}{2}(-\frac{1+3+5+7/2}{2}) = -\frac{25}{8}$, so $h_\alpha = -3 + \frac{25}{8} = \frac{1}{8}$. For comparison, from the CFT description, the $e/4$ quasihole operator is expressed as $\sigma e^{i\sqrt{2}\phi/4}$, where σ is the Majorana fermion field of Ising CFT and ϕ is the free chiral boson field. The σ operator has a conformal dimension $h = 1/16$ and thus the total dimension is $h_\alpha = 1/16 + \frac{(\sqrt{2}/4)^2}{2} = 1/8$.

For the $e/4$ excitation in the $3\bar{3}1$ state, we obtain its conformal dimension from the CFT correlator.

The ground-state wave function could be written as [59]

$$\begin{aligned}
\psi_{331}(\{z^\uparrow\}, \{z^\downarrow\}) &= \langle V^+(\{z_1^\uparrow\}) \cdots V^+(\{z_N^\uparrow\}) V^-(\{z_1^\downarrow\}) \cdots V^-(\{z_N^\downarrow\}) \rangle_{\text{spin}} \left\langle \prod_{i=1}^{2N} e^{i\sqrt{\alpha}\phi_c(z_i)} \mathcal{O}_{bg} \right\rangle_{\text{charge}} \\
&\simeq \prod_{1 \leq i < j \leq N} (z_i^\uparrow - z_j^\uparrow)^\beta \prod_{1 \leq i < j \leq N} (z_i^\downarrow - z_j^\downarrow)^\beta \prod_{i,j}^N (z_i^\uparrow - z_j^\downarrow)^{-\beta} \prod_{1 \leq i < j \leq 2N} (z_i - z_j)^\alpha \\
&\simeq \prod_{1 \leq i < j \leq N} (z_i^\uparrow - z_j^\uparrow)^{\alpha+\beta} \prod_{1 \leq i < j \leq N} (z_i^\downarrow - z_j^\downarrow)^{\alpha+\beta} \prod_{i,j}^N (z_i^\uparrow - z_j^\downarrow)^{\alpha-\beta}, \tag{D6}
\end{aligned}$$

where the spin vertex operators are $V^\pm(z) = e^{\pm i\sqrt{\beta}\phi_s(z)}$ and \mathcal{O}_{bg} is the background charge. Here the Gaussian factor has been neglected. For the 331 state, $\alpha = 2$, $\beta = 1$ and thus the electron operator (carrying charge e and spin $1/2$) is

$$V^\pm(z) e^{i\sqrt{\alpha}\phi_c(z)} = e^{\pm i\phi_s(z)} e^{i\sqrt{2}\phi_c(z)}. \tag{D7}$$

The Abelian $e/4$ quasihole is written as $e^{\pm i\frac{1}{2}\phi_s(z)} e^{i\frac{\sqrt{2}}{4}\phi_c(z)}$, which has conformal dimension

$$h = \frac{1}{2} \left(\frac{1}{2} \right)^2 + \frac{1}{2} \left(\frac{\sqrt{2}}{4} \right)^2 = \frac{3}{16}. \tag{D8}$$

The $e/4$ quasihole wave function (with a Laughlin quasihole in the \uparrow layer) can be written with chiral CFT correlator

$$\begin{aligned}
\psi_{331}(w, \{z^\uparrow\}, \{z^\downarrow\}) &= \left\langle e^{i\frac{1}{2}\phi_s(w)} e^{i\frac{\sqrt{2}}{4}\phi_c(w)} V^+(\{z_1^\uparrow\}) \cdots V^+(\{z_N^\uparrow\}) V^-(\{z_1^\downarrow\}) \cdots V^-(\{z_N^\downarrow\}) \prod_{i=1}^{2N} e^{i\sqrt{2}\phi_c(z_i)} \mathcal{O}_{bg} \right\rangle \\
&\simeq \prod_{i=1}^N (w - z_i^\uparrow)^{1/2} \prod_{i=1}^N (w - z_i^\downarrow)^{-1/2} \prod_{j=1}^{2N} (w - z_j)^{1/2} \prod_{1 \leq i < j \leq N} (z_i^\uparrow - z_j^\uparrow)^3 \prod_{1 \leq i < j \leq N} (z_i^\downarrow - z_j^\downarrow)^3 \prod_{i,j=1}^N (z_i^\uparrow - z_j^\downarrow) \\
&= \prod_{i=1}^N (w - z_i^\uparrow) \prod_{1 \leq i < j \leq N} (z_i^\uparrow - z_j^\uparrow)^3 \prod_{1 \leq i < j \leq N} (z_i^\downarrow - z_j^\downarrow)^3 \prod_{i,j=1}^N (z_i^\uparrow - z_j^\downarrow), \tag{D9}
\end{aligned}$$

which demonstrates that a Laughlin quasihole in the upper layer has been created.

APPENDIX E: $e/4$ QUASIHOLE STATE ON CYLINDER

Due to the pairing nature of the Majorana mode, we can only create even number of $e/4$ quasiholes in the MR state. For the MR state, creating one $e/4$ at w means putting another at infinity. Its wave function is

$$|\psi_{5/2}^c\rangle = \text{Pf} \left(\frac{\exp(\gamma \mathbf{z}_i) - \exp(\gamma \mathbf{w}) + \exp(\gamma \mathbf{z}_j) - \exp(\gamma \mathbf{w})}{\exp(\gamma \mathbf{z}_i) - \exp(\gamma \mathbf{z}_j)} \right) \prod_{j < k} (\exp(\gamma \mathbf{z}_j) - \exp(\gamma \mathbf{z}_k))^2 e^{-\frac{1}{2} \sum_{i=1}^N x_i^2} e^{-\sum_i (N-1) \gamma \mathbf{z}_i}. \tag{E1}$$

If we consider a pair of $e/4$ quasiholes at w_1 and w_2 , the wave function is

$$\begin{aligned}
|\psi_{5/2}^c\rangle &= \text{Pf} \left(\frac{(\exp(\gamma \mathbf{z}_i) - \exp(\gamma \mathbf{w}_1))(\exp(\gamma \mathbf{z}_j) - \exp(\gamma \mathbf{w}_2)) + (\exp(\gamma \mathbf{z}_i) - \exp(\gamma \mathbf{w}_2))(\exp(\gamma \mathbf{z}_j) - \exp(\gamma \mathbf{w}_1))}{\exp(\gamma \mathbf{z}_i) - \exp(\gamma \mathbf{z}_j)} \right) \\
&\times \prod_{j < k} (\exp(\gamma \mathbf{z}_j) - \exp(\gamma \mathbf{z}_k))^2 e^{-\frac{1}{2} \sum_{i=1}^N x_i^2} e^{-\sum_i (N-1) \gamma \mathbf{z}_i}. \tag{E2}
\end{aligned}$$

For the $e/4$ quasihole in the \uparrow layer of the 331 state, the wave function is

$$\begin{aligned}
|\psi_{331}\rangle &= \prod_{i \in N_1} (\exp(\gamma \mathbf{z}_i) - \exp(\gamma \mathbf{w})) \prod_{i < j, i, j \in N_1} (\exp(\gamma \mathbf{z}_i) - \exp(\gamma \mathbf{z}_j))^3 \prod_{k < l, k, l \in N_2} (\exp(\gamma \mathbf{z}_k) - \exp(\gamma \mathbf{z}_l))^3 \\
&\times \prod_{i \in N_1, k \in N_2} (\exp(\gamma \mathbf{z}_i) - \exp(\gamma \mathbf{z}_k)) e^{-\frac{1}{2} \sum_{i=1}^N x_i^2} \cdot e^{-\sum_{i \in N_1} \frac{\gamma}{2} (4N_1 - 2) \mathbf{z}_i - \sum_{i \in N_2} \frac{\gamma}{2} (4N_2 - 2) \mathbf{z}_i}. \tag{E3}
\end{aligned}$$

- [1] D. C. Tsui, H. L. Stormer, and A. C. Gossard, *Phys. Rev. Lett.* **48**, 1559 (1982).
- [2] R. B. Laughlin, *Phys. Rev. Lett.* **50**, 1395 (1983).
- [3] X. G. Wen and Q. Niu, *Phys. Rev. B* **41**, 9377 (1990).
- [4] X. G. Wen, *Adv. Phys.* **44**, 405 (1995).
- [5] D. Arovas, J. R. Schrieffer, and F. Wilczek, *Phys. Rev. Lett.* **53**, 722 (1984).
- [6] F. D. M. Haldane and E. H. Rezayi, *Phys. Rev. B* **31**, 2529 (1985).
- [7] H. Bartolomei, M. Kumar, R. Bisognin, A. Marguerite, J.-M. Berroir, E. Bocquillon, B. Plaçais, A. Cavanna, Q. Dong, U. Gennser, Y. Jin, and G. Fève, *Science* **368**, 173 (2020).
- [8] J. Nakamura, S. Liang, G. C. Gardner, and M. J. Manfra, *Nat. Phys.* **16**, 931 (2020).
- [9] J. Y. M. Lee and H. S. Sim, *Nat. Commun.* **13**, 6660 (2022).
- [10] R. L. Willett, K. Shtengel, C. Nayak, L. N. Pfeiffer, Y. J. Chung, M. L. Peabody, K. W. Baldwin, and K. W. West, *Phys. Rev. X* **13**, 011028 (2023).
- [11] P. Glidic, O. Maillet, A. Aassime, C. Piquard, A. Cavanna, U. Gennser, Y. Jin, A. Anthore, and F. Pierre, *Phys. Rev. X* **13**, 011030 (2023).
- [12] X. G. Wen, *Phys. Rev. B* **40**, 7387 (1989).
- [13] A. H. MacDonald, *Phys. Rev. Lett.* **64**, 220 (1990).
- [14] X. G. Wen, *Phys. Rev. B* **41**, 12838 (1990).
- [15] X. G. Wen, *Int. J. Mod. Phys. B* **06**, 1711 (1992).
- [16] M. Hilke, D. C. Tsui, M. Grayson, L. N. Pfeiffer, and K. W. West, *Phys. Rev. Lett.* **87**, 186806 (2001).
- [17] A. M. Chang, L. N. Pfeiffer, and K. W. West, *Phys. Rev. Lett.* **77**, 2538 (1996).
- [18] M. Grayson, D. C. Tsui, L. N. Pfeiffer, K. W. West, and A. M. Chang, *Phys. Rev. Lett.* **80**, 1062 (1998).
- [19] A. M. Chang, M. K. Wu, C. C. Chi, L. N. Pfeiffer, and K. W. West, *Phys. Rev. Lett.* **86**, 143 (2001).
- [20] A. M. Chang, *Rev. Mod. Phys.* **75**, 1449 (2003).
- [21] M. Grayson, *Solid State Commun.* **140**, 66 (2006).
- [22] S. S. Mandal and J. K. Jain, *Solid State Commun.* **118**, 503 (2001).
- [23] X. Wan, K. Yang, and E. H. Rezayi, *Phys. Rev. Lett.* **88**, 056802 (2002).
- [24] X. Wan, F. Evers, and E. H. Rezayi, *Phys. Rev. Lett.* **94**, 166804 (2005).
- [25] V. J. Goldman and E. V. Tsiper, *Phys. Rev. Lett.* **86**, 5841 (2001).
- [26] C. de C. Chamon and X.-G. Wen, *Phys. Rev. B* **49**, 8227 (1994).
- [27] K. Yang, *Phys. Rev. Lett.* **91**, 036802 (2003).
- [28] Y. N. Joglekar, H. K. Nguyen, and G. Murthy, *Phys. Rev. B* **68**, 035332 (2003).
- [29] Z.-X. Hu, R. N. Bhatt, X. Wan, and K. Yang, *Phys. Rev. Lett.* **107**, 236806 (2011).
- [30] S. K. Srivastav, R. Kumar, C. Spånslätt, K. Watanabe, T. Taniguchi, A. D. Mirlin, Y. Gefen, and A. Das, *Phys. Rev. Lett.* **126**, 216803 (2021).
- [31] S. K. Srivastav, R. Kumar, C. Spånslätt, K. Watanabe, T. Taniguchi, A. D. Mirlin, Y. Gefen, and A. Das, *Nat. Commun.* **13**, 5185 (2022).
- [32] R. Kumar, S. K. Srivastav, C. Spånslätt, K. Watanabe, T. Taniguchi, Y. Gefen, A. D. Mirlin, and A. Das, *Nat. Commun.* **13**, 213 (2022).
- [33] X. G. Wen, *Phys. Rev. B* **43**, 11025 (1991).
- [34] T. Ito and N. Shibata, *Phys. Rev. B* **103**, 115107 (2021).
- [35] Y. J. Park and F. D. M. Haldane, *Phys. Rev. B* **90**, 045123 (2014).
- [36] F. D. M. Haldane, *arXiv:0906.1854v1*.
- [37] J. E. Avron, R. Seiler, and P. G. Zograf, *Phys. Rev. Lett.* **75**, 697 (1995).
- [38] N. Read, *Phys. Rev. B* **79**, 045308 (2009).
- [39] H.-H. Tu, Y. Zhang, and X.-L. Qi, *Phys. Rev. B* **88**, 195412 (2013).
- [40] L. D. Hu and W. Zhu, *Phys. Rev. B* **105**, 165145 (2022).
- [41] M. P. Zaletel, R. S. K. Mong, and F. Pollmann, *Phys. Rev. Lett.* **110**, 236801 (2013).
- [42] L. Hu, Z. Liu, D. N. Sheng, F. D. M. Haldane, and W. Zhu, *Phys. Rev. B* **103**, 085103 (2021).
- [43] E. Keski-Vakkuri and X.-G. Wen, *Int. J. Mod. Phys. B* **07**, 4227 (1993).
- [44] I. Affleck, *Phys. Rev. Lett.* **56**, 746 (1986).
- [45] L. Alvarez-Gaumé and E. Witten, *Nucl. Phys. B* **234**, 269 (1984).
- [46] R. Morf and B. I. Halperin, *Phys. Rev. B* **33**, 2221 (1986).
- [47] S. Mitra and A. H. MacDonald, *Phys. Rev. B* **48**, 2005 (1993).
- [48] U. Khanna, M. Goldstein, and Y. Gefen, *Phys. Rev. B* **103**, L121302 (2021).
- [49] S. Jansen, E. H. Lieb, and R. Seiler, *Commun. Math. Phys.* **285**, 503 (2009).
- [50] D. J. Thouless, *Surf. Sci.* **142**, 147 (1984).
- [51] J. K. Jain, *Composite Fermions* (Cambridge University Press, Cambridge, 2007).
- [52] F. D. M. Haldane, *Phys. Rev. Lett.* **107**, 116801 (2011).
- [53] B. A. Bernevig and F. D. M. Haldane, *Phys. Rev. Lett.* **100**, 246802 (2008).
- [54] B. A. Bernevig and F. D. M. Haldane, *Phys. Rev. Lett.* **101**, 246806 (2008).
- [55] J. M. Luttinger, *Phys. Rev.* **119**, 1153 (1960).
- [56] X. Lin, C. Dillard, M. A. Kastner, L. N. Pfeiffer, and K. W. West, *Phys. Rev. B* **85**, 165321 (2012).
- [57] H. L. Fu, P. J. Wang, P. J. Shan, L. Xiong, L. N. Pfeiffer, K. West, M. A. Kastner, and X. Lin, *Proc. Natl. Acad. Sci. USA* **113**, 12386 (2016).
- [58] M. Wimmer, *ACM Trans. Math. Software* **38**, 1 (2012).
- [59] G. Moore and N. Read, *Nucl. Phys. B* **360**, 362 (1991).